Probing the Combined Electromagnetic Local Density of Optical States with Quantum Emitters Supporting Strong Electric and Magnetic Transitions

Dongfang Li,[*] Sinan Karaveli,[*] Sébastien Cueff,[†] Wenhao Li, and Rashid Zia[‡]

School of Engineering and Department of Physics, Brown University, Providence, Rhode Island 02912, USA

We experimentally demonstrate that the radiative decay rate of a quantum emitter is determined by the combined electric and magnetic local density of optical states (LDOS). A Drexhage-style experiment was performed for two distinct quantum emitters, divalent nickel ions in magnesium oxide and trivalent erbium ions in yttrium oxide, which both support nearly equal mixtures of isotropic electric dipole and magnetic dipole transitions. The disappearance of lifetime oscillations as a function of emitter-interface separation distance confirms that the electromagnetic LDOS refers to the total mode density, and thus similar to thermal emission, these unique electronic emitters effectively excite all polarizations and orientations of the electromagnetic field.

The advent of metamaterials has helped to highlight the diversity of electromagnetic resonances in optical nano-structures. For example, recent studies have shown how the interplay of electric and magnetic resonances can enable exciting new effects, such as zero optical backscattering [1–4], enhanced chiral spectroscopy [5], and robust optical activity [6]. The interaction of electric and magnetic resonances has also been used to reproduce phenomena from atomic physics, e.g., Fano resonances [7–11]. In this regard, there are strong similarities between the lifetime of microscopic quantum emitters and the linewidth of macroscopic scatterers [12], but there are also intriguing differences. Recent calculations have revealed that the scattering linewidth of a split-ring resonator should follow a newly defined magnetoelectric local density of optical states (LDOS) that emerges from cross-coupling of its electric and magnetic resonances [13].

Although the term LDOS is widely used in nano-optics [14–16], its precise definition can be elusive [17,18]. Within a bulk (homogeneous) medium, the volume density of electromagnetic modes is a well-defined, spatially uniform quantity that plays an important role, for example, in the analysis of blackbody emission [19,20]. Within structured optical environments though, the density and accessibility of modes can vary with position, hence the term LDOS. The effect of this variation can be seen in the modified lifetimes of electronic emitters near surfaces, as demonstrated in Drexhage's pioneering experiments [21]. Since most common emitters are dominated by electric dipole (ED) transitions, the term LDOS has become almost synonymous with the electric LDOS [16–18].

Recent research has also helped highlight the diversity of electronic transitions in quantum emitters. For example, there has been renewed interest in the magnetic dipole (MD) transitions of lanthanide and transition-metal ions, whose emission rates scale with the magnetic LDOS [22–35]. Nevertheless, these MD transitions are often accompanied by dominant ED transitions that originate from the same excited state. Consequently, their lifetimes are still primarily determined by the electric LDOS [21,31,36], and most research has focused instead on using branching ratios of spectrally distinct ED and MD emission lines as a means to investigate the relative electric and magnetic contributions to LDOS [23,24,32,34,35]. Interestingly, even for strongly mixed ED and MD emitters (e.g., trivalent erbium ions [37]), lifetime data are generally interpreted by a purely ED model in previous studies [14,38,39].

In canonical Drexhage-style experiments, the lifetime of a quantum emitter placed near an interface can be expressed as follows [36]:

$$\tau(d) = \tau_0\{1 - q[1 - \tilde{\Gamma}(d)]\}^{-1}, \qquad (1)$$

where d is the separation distance between the emitter and the interface, q and τ_0 correspond to the emitter's quantum efficiency and lifetime in a homogenous medium, respectively, and where $\tilde{\Gamma}(d) \equiv \Gamma(d)/\Gamma_0$ is the normalized LDOS, i.e., the radiative decay rate normalized to the homogeneous case. In the literature [14,21,36,40], the lifetime values of purely ED emitters placed at different distances away from an interface are commonly used to probe the electric LDOS with the lifetime oscillations being fit to infer quantum efficiency (Fig. 1). However, these oscillations in the electric (or magnetic) LDOS are not a fundamental feature of the electromagnetic mode density; they represent the differing interference patterns associate with electric (or magnetic) fields near a surface. The commonly measured electric LDOS is only the projection of the combined electromagnetic LDOS onto an isotropic electric dipole [Fig. 1(a)]. Therefore, one would predict that
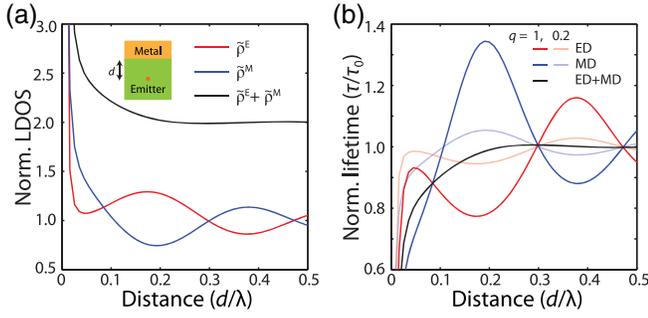
FIG. 1. (a) Normalized electric ($\tilde{\rho}^E$, red) and magnetic ($\tilde{\rho}^M$, blue) LDOS together with their summation ($\tilde{\rho}^E + \tilde{\rho}^M$, black). Inset is the sample schematic. (b) Normalized lifetimes for purely ED (red), MD (blue), and strongly mixed ED-MD emitters (black) with varied quantum efficiencies q. The dielectric constants for the emitter's host and metal are $\epsilon = 2.25$ and $-97 + 11.5i$.

a strongly mixed ED-MD emitter probing the combined electromagnetic LDOS would exhibit a fundamentally different lifetime dependence.

In this Letter, we experimentally investigate this question using two strongly mixed ED-MD emitters based on both transition-metal and lanthanide ions: divalent-nickel-doped magnesium oxide ($Ni^{2+}:MgO$) and trivalent-erbium-doped yttrium oxide ($Er^{3+}:Y_2O_3$). We first quantify the ED and MD contributions to the near-infrared emission of $Ni^{2+}:MgO$ for the $^3T_2 \rightarrow {}^3A_2$ band using energy-momentum spectroscopy [27], and experimentally demonstrate that MD transitions account for ~50% of the total intrinsic emission. We then demonstrate that the lifetime of this mixed ED-MD emitter near metal and dielectric interfaces does not solely depend on the electric or magnetic LDOS, but rather follows the combined electromagnetic LDOS. This is further confirmed by the strongly mixed ED-MD transition of Er^{3+} ions ($^4I_{13/2} \rightarrow {}^4I_{15/2}$) at telecommunication wavelengths, while the ED transitions in the visible regime ($^4S_{3/2} \rightarrow {}^4I_{15/2}$) originating from the same Er^{3+} ions solely depend on the electric LDOS. These results show that strongly mixed ED-MD emitters can probe the total LDOS much like a thermal emitter [17], and we discuss the implications for measurements of the local electromagnetic mode density.

The $Ni^{2+}:MgO$ emitter layer was fabricated on top of a quartz coverslip by sequential electron beam evaporation of ~18 nm of MgO, ~1 nm of Ni^{2+}-doped (1 at.%) MgO, and ~18 nm MgO. The sample was subsequently annealed at 1000 °C for 1 h to diffuse the Ni^{2+} ions throughout the layer and thus reduce the doping concentration. For energy-momentum characterization, a 401 nm diode laser was focused to the back-focal-plane of a 1.3 numerical aperture (NA) microscope objective beyond the critical angle in the so-called total internal reflection fluorescence mode. A linear polarizer and 100 mm Bertrand lens were used

to project polarized momentum-space emission patterns onto the entrance slit of an imaging spectrograph equipped with a 2D InGaAs detector array (Princeton Instruments, Isoplane SCT 320 with NIRvana), as shown in Fig. 2(a).

As discussed in detail in Ref. [27], this analysis allows us to obtain the intrinsic spectrally resolved ED and MD emission rates [Fig. 2(b)] that would be observed in a bulk homogeneous medium [41]. Note that the ~400 cm^{-1} energy separation between the MD and ED emission rate maxima is consistent with the average phonon energy in MgO [56], suggesting that ED and MD transitions are distinguished by a single phonon process. Most importantly for this study, the rates shown in Fig. 2(b) indicate that this broadband emission has a strongly mixed ED and MD character. Integrating over these spectrally resolved rates, we find that MD transitions account for approximately half (50.4 ± 2.5%) of the total emission rate for the $^3T_2 \rightarrow {}^3A_2$ band. To demonstrate that the $^3T_2 \rightarrow {}^3A_2$ transition depends on the total electromagnetic LDOS and, thus, that $Ni^{2+}:MgO$ serves as a quantum mechanical probe of the local electromagnetic mode density, we have performed lifetime experiments to study the modified spontaneous emission rates near planar interfaces.
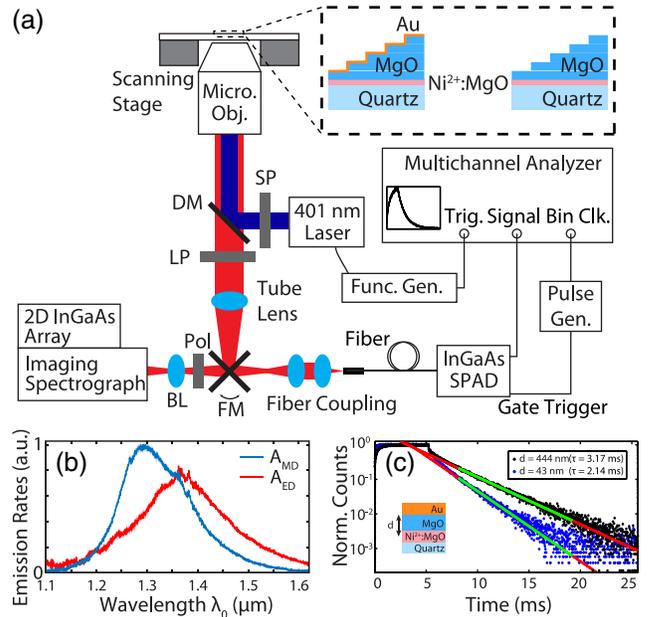
FIG. 2. (a) Schematic of experimental setup. BL: Bertrand lens, DM: Dichroic mirror, LP: Long pass filter, Pol: Linear polarizer, SP: Short pass filter. Flip mirror (FM) switches between the energy-momentum spectroscopy setup (left) and the lifetime measurement setup (right). Inset depicts the MgO steps separating the $Ni^{2+}:MgO$ emitter layer from either gold mirror or air interface for the lifetime studies. (b) Spectrally-resolved emission rates, A_{ED} (red line) and A_{MD} (blue line), deduced from fitting analysis together with 95% confidence intervals (shaded regions). (c) Examples of time-resolved photoluminescence data and fits used to determine the excited state lifetime.

For the lifetime study, we varied the distance of the Ni^{2+}:MgO thin film to both a gold mirror and an air interface, and acquired time-decay traces of its photoluminescence. For this purpose, different thickness spacers were fabricated by consecutive evaporation of undoped MgO while masking parts of the sample to achieve ~2 mm wide steps with heights ranging from ~25 to ~475 nm. Then, a gold mirror was deposited on a portion of each step by evaporating a 5 nm Ti adhesion layer followed by 200 nm of Au. Schematic illustrations of the final structures are shown in the inset of Fig. 2(a). The sample was excited, and emission collected, with a 20× (0.75 NA) microscope objective under confocal illumination. The 401 nm diode laser was modulated using a function generator to pump the emitters. As shown in Fig. 2(a), the collected emission was focused into a fiber coupled InGaAs/InP near-infrared single photon avalanche photodiode (SPAD) detector module (Micro Photon Devices) [57]. Histograms of photon arrival times were obtained using a multichannel analyzer (Stanford Research Systems, SR430). (See Supplemental Material for more details [41].) Example time decay traces for two different spacer layer thicknesses are shown in Fig. 2(c) together with fit results to a single exponential decay. As highlighted by green lines in Fig. 2(c), all fits were performed over the same time region between 3 and 14 ms after the excitation pulse ends to isolate the excited state lifetime of the long-lived $^3T_2$ state.

Figure 3 shows the measured lifetimes as a function of distance d from the center of the Ni^{2+}:MgO thin film to the gold and air interfaces. Note that the lifetimes do not exhibit large oscillations, as would be expected for dominantly ED or MD transitions (see Fig. 1). Instead, Fig. 3(a) shows a steep rise in the lifetime followed by a gentle increase as the emitter-mirror separation is increased, whereas for increasing distances from the air interface, Fig. 3(b) shows a decrease toward a plateau.

The lifetime values shown in Fig. 3 cannot be fit to purely ED or purely MD emitters. Although one might assume that the relative absence of oscillations could be attributed to a low quantum efficiency, this cannot account for the large variations observed near the air interface. To demonstrate this point, the red line in Fig. 3 shows the best least-squares fit obtained using Eq. (1) and assuming an isotropic purely ED emitter with τ_0 and q as fit parameters. This ED fit clearly does not follow the observed data, especially at short distances from the gold mirror, for which ED emission should be inhibited by interference effects but our measurements show a marked decrease in lifetime. (See Supplemental Material for more details [41].)

The measured lifetimes can be fit to a superposition of isotropic ED and MD emission. To do so we set $\tilde{\Gamma}(d) \equiv a_{MD}\tilde{\Gamma}_{MD}^{Iso}(d) + (1 - a_{MD})\tilde{\Gamma}_{ED}^{Iso}(d)$, where a_{MD} is the MD percentage of total emission that we use as a fit variable parameter together with τ_0 in Eq. (1). Here $\tilde{\Gamma}_{ED}^{Iso}(d) \equiv \tilde{\rho}^E(d) = \rho^E/\rho_0^E$ and $\tilde{\Gamma}_{MD}^{Iso}(d) \equiv \tilde{\rho}^M(d) = \rho^M/\rho_0^M$ are the
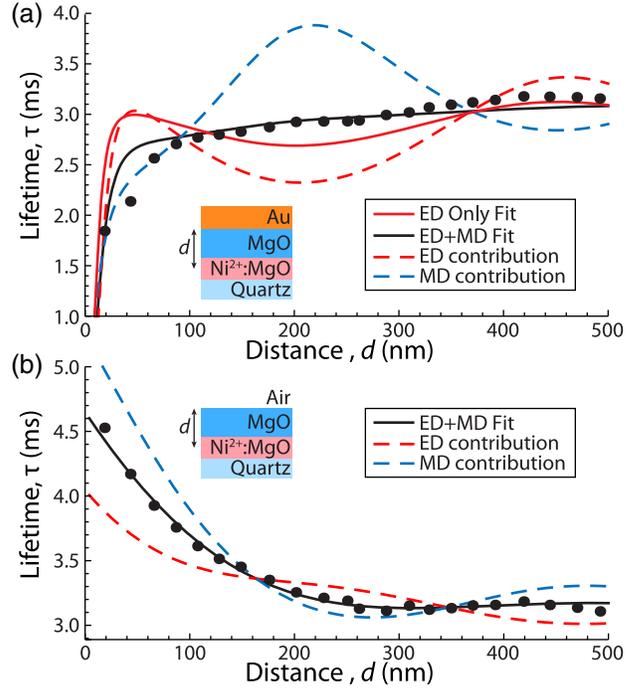
FIG. 3. Lifetime data acquired for $^3T_2$ state of Ni^{2+}:MgO near (a) a gold mirror and (b) an air interface together with fits to the purely electric LDOS (red solid line) and combined electromagnetic LDOS (black line). For completeness, we also plot the electric (red dashed) and magnetic (blue dashed) contributions to the electromagnetic LDOS, i.e., the variations expected for ED and MD transitions which are then averaged according to the fit percentages to obtain the black curve. Error bars associated with measured lifetimes are not shown here, because they are smaller than the data point symbols.

normalized electric and magnetic LDOS, respectively [41]. To reduce the number of fit parameters, we leverage the fact that the quantum efficiency is defined by: $q = \tau_0/\tau_{rad}$, where $\tau_{rad} = 3.6$ ms is the intrinsic radiative lifetime of the $^3T_2 \rightarrow {}^3A_2$ transition of Ni^{2+}:MgO inferred from temperature dependent measurements [58]. The resulting fits are shown by the black lines in Figs. 3(a) and 3(b). For the gold case, we obtain $\tau_0 = 2.72 \pm 0.06$ ms and $a_{MD} = 52.4 \pm 8.2\%$, and these results agree well with the experimental lifetime data. For completeness, the dashed lines in Fig. 3 show the calculated lifetime variations associated with the ED and MD contributions. Similar fitting analysis for the air case yields $\tau_0 = 2.81 \pm 0.01$ ms and $a_{MD} = 56.9 \pm 4.8\%$. The a_{MD} values obtained from both sets of lifetime measurements agree well with the energy-momentum characterization.

For the special case where the intrinsic ED and MD rates are identical (i.e., $a_{MD} = 50\%$), the normalized radiative decay rate $\tilde{\Gamma}$ scales with the combined electromagnetic LDOS,

$$\tilde{\rho}^{EM}(d) = \frac{\rho^E(d) + \rho^M(d)}{\rho_0^E + \rho_0^M} = \frac{1}{2}[\tilde{\rho}^E(d) + \tilde{\rho}^M(d)], \quad (2)$$

by noting the fact that $\rho_0^E = \rho_0^M$ in a bulk medium [17,18]. Applying Eq. (2) to Eq. (1), we can further derive that

$$\tilde{\rho}^{EM}(d) = \frac{\tau_0}{q\tau(d)} + 1 - \frac{1}{q}. \qquad (3)$$

Therefore, by employing emitters with roughly equal ED and MD emission rates as well as characterized quantum efficiency and bulk lifetime, a single lifetime measurement can be used to probe $\tilde{\rho}^{EM}$ (i.e., the normalized electromagnetic mode density that can be accessed) at the position of interest in a complex optical system. Unlike $\tilde{\rho}^E$ and $\tilde{\rho}^M$, this quantity is less sensitive to far-field interference, i.e., the spatial variations between electric and magnetic field maxima (Fig. 1). However, it is still very sensitive to near-field phenomena. Indeed, in Fig. 3, we see the ∼3 ms lifetime observed far from both interfaces increases by ∼50% near the air surface and decreases by ∼40% near the gold mirror. These large changes result from the decreased mode density near the low index air and the increased contributions of surface modes near the gold film.

A more common emitter with mixed ED-MD transitions is $Er^{3+}:Y_2O_3$, where it was recently shown that the technologically important 1.5 μm transition ${}^4I_{13/2} \rightarrow {}^4I_{15/2}$ has nearly equal ED and MD contributions [59–61]. To explore this emitter system we fabricated a similar staircaselike sample with 44 distinct regions (i.e., different thickness spacers and/or top interfaces). The photoluminescence time-decay traces for the ${}^4I_{13/2} \rightarrow {}^4I_{15/2}$ transition at telecom wavelengths were measured using a setup similar to that shown in Fig. 2(a) with a mechanically chopped 532 nm excitation laser. The obtained lifetime data are shown by black dots in Fig. 4.

Since the intrinsic MD radiative rate for the ${}^4I_{13/2} \rightarrow {}^4I_{15/2}$ transition of $Er^{3+}:Y_2O_3$ can be directly obtained from free-ion calculations ($\Gamma_0^{MD} = 1.74^3 \times 10.17 \text{ s}^{-1} = 53.6 \text{ s}^{-1}$) [28], Eq. (1) can be rewritten as

$$\tau(d) = [\Gamma_{nr} + \Gamma_0^{ED}\tilde{\Gamma}_{ED}^{Iso}(d) + \Gamma_0^{MD}\tilde{\Gamma}_{MD}^{Iso}(d)]^{-1}, \qquad (4)$$

where Γ_{nr} is the nonradiative decay rate, Γ_0^{ED} and Γ_0^{MD} are the spontaneous emission rates of ED and MD in a homogeneous medium. We then fit the measured data using Eq. (4) with only two free parameters Γ_{nr} and Γ_0^{ED}. The black lines in Fig. 4 show the resulting fits, which agree well with experimental results, except for the two closest distances to the gold film which have been purposely excluded from fitting procedure (see Supplemental Material for more details [41]). The fit parameters are extracted to be $\Gamma_0^{ED} = 80 \pm 7$ and $\Gamma_{nr} = 32 \pm 6 \text{ s}^{-1}$. These values correspond to a quantum efficiency q of $81 \pm 6\%$ and radiative lifetime τ_{rad} of 7.5 ± 0.4 ms at room temperature, which is consistent with the lifetime of 8.0 ± 0.5 ms measured at low temperature [37]. The fractional contribution of MD emission a_{MD}
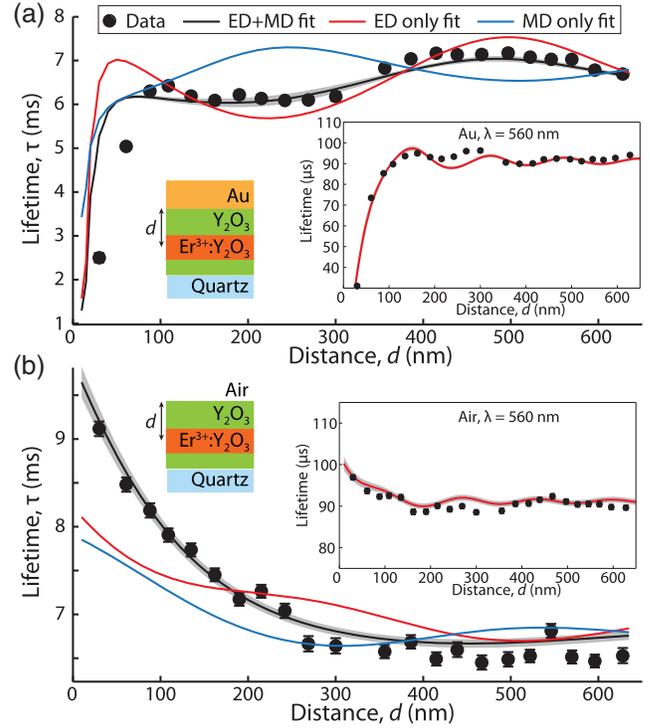
FIG. 4. Fits of the lifetime data by the mixed ED-MD model (black line), the purely ED model (red line) and the purely MD model (blue line) for both cases: with the gold mirror (a) and with an air interface (b). The shaded gray area represents the 95% confidence intervals of fitting result in the ED and MD model. The insets show the lifetime data together with a purely ED model fit of the ${}^4S_{3/2} \rightarrow {}^4I_{15/2}$ transition at wavelength ∼560 nm measured on the same sample, which yields $\tau_0 = 89 \pm 0.7$ μs and $q = 35.9 \pm 5.2\%$.

is calculated to be $40 \pm 2\%$, which is comparable with the result extracted using energy-momentum spectroscopy (∼46%) [41]. The minor deviation may originate from the residual energy transfer between adjacent Er^{3+} ions causing lifetime changes [62]. To further confirm the mixed nature of this transition, red lines in Fig. 4 show fits to the lifetime data for both cases to a purely ED model (i.e., $\Gamma_0^{MD} = 0$), which is widely used in previous studies [14,38,39]. The ED fitting results clearly deviates from the experimental data. Deviations are observed as well for fitting to a purely MD model (i.e., $\Gamma_0^{ED} = 0$), as shown by the blue lines in Fig. 4.

In addition to the mixed ED-MD telecom transitions, Er^{3+} ions support strong ED emission lines at visible wavelengths that are commonly used in up-conversion applications [63]. Taking advantage of this property, we studied the visible fluorescence of our sample under 980-nm laser excitation to avoid gold fluorescence. Using a bandpass filter and silicon SPAD (PicoQuant, τ-SPAD), we examined the lifetime oscillations of the ${}^4S_{3/2} \rightarrow {}^4I_{15/2}$ ED transition near 560 nm [37]. The insets in Fig. 4 demonstrate that data measured for both air and Au interfaces can

be well fitted by a purely ED model. In contrast to the mixed ED-MD telecom emission, the suppressed oscillations in this visible ED emission can be well explained by the low quantum efficiency (i.e., ∼36%) [64].

In conclusion, we have demonstrated that strongly mixed ED and MD emitters probe the combined electric and magnetic LDOS, i.e., the electromagnetic LDOS experienced by an incoherent sum of ED and MD transitions. These results have important implications for experiments and proposals to use MD emission in transition-metal and lanthanide ions to probe magnetic field effects [32–35], because such MD emission is often accompanied by ED transitions of comparable or greater probability. Interestingly, this electromagnetic LDOS is the same quantity probed by thermal emission [17]. In this context, these results complement recent work on thermal radiation scanning tunneling microscopy (TRSTM) [65–67] and may provide a new experimental system with which to study near-field radiative heat transfer [68]. Similar to thermal emission, such measurements based on strongly mixed ED-MD transitions could allow one to isolate and investigate thermal-like radiation effects without the need to heat samples nor minimize other thermal transport channels (i.e., conduction and convection). Lifetime measurements with these isotropic emitters also probe all components of the electromagnetic LDOS, unlike TRSTM scattering measurements which probe a projection of the LDOS along the tip axis [65].

More generally, the study of these and other multipolar emitters may help broaden the range of electromagnetic phenomena that can be accessed with electronic systems. Having identified emitters with near-equal incoherent ED and MD contributions, an open question remains as to whether these or other solid-state materials can be engineered to exhibit a coherent superposition of near-equal ED and MD transitions. Such emitters could help realize atomic analogues to the recent phenomena explored with macroscopic ED and MD scatterers [1–6].

---

*D. L. and S. K. contributed equally to this work.
†Present address: Institut des Nanotechnologies de Lyon, Ecole Centrale de Lyon, 69134 Ecully, France.
‡Rashid_Zia@brown.edu

[1] J. M. Geffrin *et al.*, Nat. Commun. **3**, 1171 (2012).
[2] Y. H. Fu, A. I. Kuznetsov, A. E. Miroshnichenko, Y. F. Yu, and B. Lukyanchuk, Nat. Commun. **4**, 1527 (2013).
[3] S. Person, M. Jain, Z. Lapin, J. J. Sáenz, G. Wicks, and L. Novotny, Nano Lett. **13**, 1806 (2013).
[4] Z. Xi and H. P. Urbach, Phys. Rev. Lett. **119**, 053902 (2017).
[5] A. García-Etxarri and J. A. Dionne, Phys. Rev. B **87**, 235409 (2013).
[6] I. Sersic, M. A. van de Haar, F. B. Arango, and A. F. Koenderink, Phys. Rev. Lett. **108**, 223903 (2012).
[7] J. A. Fan, C. Wu, K. Bao, J. Bao, R. Bardhan, N. J. Halas, V. N. Manoharan, P. Nordlander, G. Shvets, and F. Capasso, Science **328**, 1135 (2010).
[8] A. B. Evlyukhin, C. Reinhardt, A. Seidel, B. S. Luk'yanchuk, and B. N. Chichkov, Phys. Rev. B **82**, 045404 (2010).
[9] B. Luk'yanchuk, N. I. Zheludev, S. A. Maier, N. J. Halas, P. Nordlander, H. Giessen, and C. T. Chong, Nat. Mater. **9**, 707 (2010).
[10] S. N. Sheikholeslami, A. García-Etxarri, and J. A. Dionne, Nano Lett. **11**, 3927 (2011).
[11] Y. Yang, W. Wang, A. Boulesbaa, I. I. Kravchenko, D. P. Briggs, A. Puretzky, D. Geohegan, and J. Valentine, Nano Lett. **15**, 7388 (2015).
[12] B. C. Buchler, T. Kalkbrenner, C. Hettich, and V. Sandoghdar, Phys. Rev. Lett. **95**, 063003 (2005).
[13] A. Kwadrin and A. F. Koenderink, Phys. Rev. B **87**, 125123 (2013).
[14] E. Snoeks, A. Lagendijk, and A. Polman, Phys. Rev. Lett. **74**, 2459 (1995).
[15] C. Chicanne, T. David, R. Quidant, J. C. Weeber, Y. Lacroute, E. Bourillot, A. Dereux, G. Colas des Francs, and C. Girard, Phys. Rev. Lett. **88**, 097402 (2002).
[16] L. Novotny and B. Hecht, *Principles of Nano-Optics* (Cambridge University Press, Cambridge, England, 2006).
[17] K. Joulain, R. Carminati, J.-P. Mulet, and J.-J. Greffet, Phys. Rev. B **68**, 245405 (2003).
[18] A. Narayanaswamy and G. Chen, J. Quant. Spectrosc. Radiat. Transfer **111**, 1877 (2010).
[19] W. Eckhardt, Opt. Commun. **41**, 305 (1982).
[20] R. Loudon, *The Quantum Theory of Light* (Oxford University Press, New York, 2000).
[21] K. H. Drexhage, Prog. Opt. **12**, 163 (1974).
[22] N. Noginova, G. Zhu, M. Mavy, and M. A. Noginov, J. Appl. Phys. **103**, 07E901 (2008).
[23] S. Karaveli and R. Zia, Opt. Lett. **35**, 3318 (2010).
[24] S. Karaveli and R. Zia, Phys. Rev. Lett. **106**, 193004 (2011).
[25] M. K. Schmidt, R. Esteban, J. J. Sáenz, I. Suárez-Lacalle, S. Mackowski, and J. Aizpurua, Opt. Express **20**, 13636 (2012).
[26] B. Rolly, B. Bebey, S. Bidault, B. Stout, and N. Bonod, Phys. Rev. B **85**, 245432 (2012).
[27] T. H. Taminiau, S. Karaveli, N. F. van Hulst, and R. Zia, Nat. Commun. **3**, 979 (2012).
[28] C. M. Dodson and R. Zia, Phys. Rev. B **86**, 125102 (2012).
[29] S. Karaveli, A. J. Weinstein, and R. Zia, Nano Lett. **13**, 2264 (2013).
[30] S. M. Hein and H. Giessen, Phys. Rev. Lett. **111**, 026803 (2013).
[31] S. Karaveli, S. Wang, G. Xiao, and R. Zia, ACS Nano **7**, 7165 (2013).
[32] L. Aigouy, A. Cazé, P. Gredin, M. Mortier, and R. Carminati, Phys. Rev. Lett. **113**, 076101 (2014).

[33] M. Kasperczyk, S. Person, D. Ananias, L. D. Carlos, and L. Novotny, Phys. Rev. Lett. **114,** 163903 (2015).

[34] F. T. Rabouw, P. T. Prins, and D. J. Norris, Nano Lett. **16,** 7254 (2016).

[35] M. Sanz-Paz, C. Ernandes, J. U. Esparza, G. W. Burr, N. F. van Hulst, A. Maitre, L. Aigouy, T. Gacoin, N. Bonod, M. F. Garcia-Parajo, S. Bidault, and M. Mivelle, Nano Lett. **18,** 3481 (2018).

[36] R. R. Chance, A. Prock, and R. Silbey, Adv. Chem. Phys. **37,** 1 (1978).

[37] M. J. Weber, Phys. Rev. **171,** 283 (1968).

[38] A. M. Vredenberg, N. E. J. Hunt, E. F. Schubert, D. C. Jacobson, J. M. Poate, and G. J. Zydzik, Phys. Rev. Lett. **71,** 517 (1993).

[39] M. J. A. de Dood, L. H. Slooff, A. Polman, A. Moroz, and A. van Blaaderen, Phys. Rev. A **64,** 033807 (2001).

[40] M. Frimmer, Y. Chen, and A. F. Koenderink, Phys. Rev. Lett. **107,** 123602 (2011).

[41] See Supplemental Material at http://link.aps.org/supplemental/10.1103/PhysRevLett.121.227403 for more details about the motivation, experimental methods, LDOS analysis, and fitting procedures, which includes Refs. [42–55].

[42] S. Sugano, Y. Tanabe, and H. Kamimura, *Multiplets of Transition-Metal Ions in Crystals* (Academic Press, New York, 1970).

[43] B. Henderson and G. F. Imbusch, *Optical Spectroscopy of Inorganic Solids* (Oxford University Press, New York, 2006).

[44] L. F. Johnson, R. E. Dietz, and H. J. Guggenheim, Phys. Rev. Lett. **11,** 318 (1963).

[45] P. F. Moulton, A. Mooradian, and T. B. Reed, Opt. Lett. **3,** 164 (1978).

[46] J. Ferguson, H. J. Guggenheim, L. F. Johnson, and H. Kamimura, J. Chem. Phys. **38,** 2579 (1963).

[47] J. E. Ralph and M. G. Townsend, J. Chem. Phys. **48,** 149 (1968).

[48] N. Manson, Phys. Rev. B **4,** 2645 (1971).

[49] B. Bird, G. Osborne, and P. Stephens, Phys. Rev. B **5,** 1800 (1972).

[50] K. Wong, D. Sengupta, and E. Krausz, Chem. Phys. Lett. **21,** 137 (1973).

[51] C. Campochiaro, D. S. McClure, P. Rabinowitz, and S. Dougal, Phys. Rev. B **43,** 14 (1991).

[52] M. J. Riley, J. Hall, and E. R. Krausz, Australian Journal of Chemistry **65,** 1298 (2012).

[53] N. Mironova-Ulmane, M. Brik, and I. Sildos, J. Lumin. **135,** 74 (2013).

[54] W. Becker, *Advanced Time-Correlated Single Photon Counting Techniques* (Springer, Berlin, Heidelberg, 2005).

[55] A. D. Rakic, A. B. Djurišic, J. M. Elazar, and M. L. Majewski, Appl. Opt. **37,** 5271 (1998).

[56] G. Peckham, Proc. Phys. Soc. **90,** 657 (1967).

[57] A. Tosi, A. Della Frera, A. B. Shehata, and C. Scarcella, Rev. Sci. Instrum. **83,** 013104 (2012).

[58] M. V. Iverson, J. C. Windscheif, and W. A. Sibley, Appl. Phys. Lett. **36,** 183 (1980).

[59] D. Li, M. Jiang, S. Cueff, C. M. Dodson, S. Karaveli, and R. Zia, Phys. Rev. B **89,** 161409 (2014).

[60] S. Cueff, D. Li, Y. Zhou, F. J. Wong, J. A. Kurvits, S. Ramanathan, and R. Zia, Nat. Commun. **6,** 8636 (2015).

[61] B. Choi, M. Iwanaga, Y. Sugimoto, K. Sakoda, and H. T. Miyazaki, Nano Lett. **16,** 5191 (2016).

[62] A. Polman, J. Appl. Phys. **82,** 1 (1997).

[63] E. M. Chan, Chem. Soc. Rev. **44,** 1653 (2015).

[64] Y. Zhanci, H. Shihua, L. Shaozhe, and C. Baojiu, J. Non-Cryst. Solids **343,** 154 (2004).

[65] Y. De Wilde, F. Formanek, R. Carminati, B. Gralak, P.-A. Lemoine, K. Joulain, J.-P. Mulet, Y. Chen, and J.-J. Greffet, Nature (London) **444,** 740 (2006).

[66] A. C. Jones and M. B. Raschke, Nano Lett. **12,** 1475 (2012).

[67] A. Babuty, K. Joulain, P.-O. Chapuis, J.-J. Greffet, and Y. De Wilde, Phys. Rev. Lett. **110,** 146103 (2013).

[68] K. Joulain, J.-P. Mulet, F. Marquier, R. Carminati, and J.-J. Greffet, Surf. Sci. Rep. **57,** 59 (2005).